

Adding Long-Wavelength Power to N-body Simulations

Shaun Cole

*Department of Physics, University of Durham, Science Laboratories, South Rd, Durham DH1 3LE.
Shaun.Cole@durham.ac.uk*

5 May 2018

ABSTRACT

Tormen & Bertschinger have presented an algorithm which allows the dynamic range of N-body simulations to be extended by adding long-wavelength power to an evolved N-body simulation. This procedure is of considerable interest as it will enable mock galaxy catalogues to be constructed with volumes as large as those of the next generation of galaxy redshift surveys. Their algorithm, however, neglects the coupling between long-wavelength linear modes and short-wavelength non-linear modes. The growth of structure on small scales is coupled to the amplitude of long-wavelength density perturbations via their effect on the local value of the density parameter Ω_0 . The effect of neglecting this coupling is quantified using a set of specially tailored N-body simulations. It is shown that the large-scale clustering of objects defined in the evolved density field such as galaxy clusters is strongly underestimated by their algorithm. An adaptation to their algorithm is proposed that, at the expense of additional complexity, remedies the shortcomings of the original one. Methods of constructing biased mock galaxy catalogues which utilise the basic algorithm of Tormen & Bertschinger, but avoid the pitfalls are discussed.

Key words: cosmology: theory – large-scale structure of Universe

1 INTRODUCTION

Tormen & Bertschinger (1996) have presented a procedure to extend the dynamic range of large cosmological N-body simulations. Their algorithm allows a periodic N-body simulation in a box of side $S \gtrsim 100h^{-1}\text{Mpc}$ to be replicated and distorted to produce a particle distribution in a larger box of side $L \gtrsim 800h^{-1}\text{Mpc}$, in which the required linear power spectrum is accurately represented in the mass distribution up to wavelengths $\lambda = L$. This procedure can therefore be used to take N-body simulations which have the mass resolution to resolve small galaxy groups and from them construct mock galaxy catalogues equal in volume to the next generation of redshift surveys, *e.g.* the Anglo-Australian 2df galaxy redshift survey (Maddox *et al.* in preparation; <http://msowww.anu.edu.au/colles/2dF/>) and the SDSS (Gunn 1995). Their method, however, neglects coupling between long-wavelength linear modes and short-wavelength non-linear modes. This coupling has only a small effect on the large scale clustering properties of the mass distribution, but a much larger effect on the large scale clustering of non-linear objects, which are highly biased tracers of the mass distribution such as galaxy clusters or perhaps galaxies. In this paper we quantify the effect of neglecting this particular form of mode coupling and suggest how the algorithm could be improved or its shortcomings circumvented.

In Section 2 we present the details of the algorithm

used to add long-wavelength power to an N-body simulations. A version of the basic algorithm developed by Tormen & Bertschinger (1996) is detailed in Section 2.1. The effect of long-wavelength linear modes on the evolution of short-wavelength non-linear modes is discussed in Section 2.2, where a modification of the basic algorithm is proposed that at the expense of additional complexity incorporates, to first order, the effect of this form of mode coupling. In Section 3 we use a set of specially tailored N-body simulations to test the basic and extended algorithms and illustrate the effect of ignoring mode coupling. In Section 4 we address the specific problem of constructing large mock galaxy catalogues in which galaxies are biased tracers of the mass distribution. We show how the shortcomings of the basic algorithm can be largely circumvented by restriction to a particular class of biasing scheme or by making a very minor modification to the basic Tormen & Bertschinger algorithm. We conclude in Section 5.

2 ADDING LONG-WAVELENGTH POWER

The procedure described by Tormen & Bertschinger (1996) and named MAP (Mode Adding Procedure) consists of the following steps. First the power in long-wavelength modes is removed from the original N-body particle positions and velocities. This new particle distribution is then replicated

arXiv:astro-ph/9604046v2 6 Sep 1996

to define a particle distribution over a much larger volume than that of the original simulation. A new density field is then generated with the required power spectrum on a finer grid in \mathbf{k} -space, but populating the same physical region of \mathbf{k} -space as the original modes that were removed. The displacements computed from this grid are then used to perturb the replicated particle positions and velocities.

An implementation of these steps is described in Section 2.1, while an additional procedure to deal with the mode coupling not considered by Tormen & Bertschinger (1996) is described in Section 2.2.

2.1 Basic Algorithm: Spatial Perturbations

The starting point of the MAP are the final positions, \mathbf{x} , and velocities, \mathbf{v} , of a large periodic N-body simulation. The size of the box, S , must be greater $\sim 100h^{-1}\text{Mpc}$ so that the evolution of the longest wavelength modes present in the box is still described well by linear theory. One also requires the corresponding linear density field, $\delta^S(\mathbf{x})$, but since only the long-wavelength contribution to this field is used this can be computed accurately from the particle positions.

The first step is to compute the long-wavelength contribution, $\Delta^S(\mathbf{x})$, to the density field $\delta^S(\mathbf{x})$. This is achieved by Fourier transforming the density field and then constructing $\Delta^S(\mathbf{x})$ using only the long-wavelength Fourier modes,

$$\Delta^S(\mathbf{x}) = \sum_{l,m,n} \delta_{\mathbf{k}}^S e^{i\mathbf{k}\cdot\mathbf{x}} \quad (2.1)$$

where $\mathbf{k} = (2\pi/S)(l, m, n)$ and $-N_S \leq l, m, n \leq N_S$. The extent of the region of \mathbf{k} -space defining $\Delta^S(\mathbf{x})$ (chosen here for simplicity to be a cube) should be limited such that $\langle |\Delta^S(\mathbf{x})|^2 \rangle \ll 1$. In practice this stage of the algorithm works accurately provided $\langle |\Delta^S(\mathbf{x})|^2 \rangle^{1/2} \lesssim 0.2$. The next step is to compute the displacements produced by these modes using the Zel'dovich (1970) approximation,

$$\mathbf{d}^S(\mathbf{x}) = \sum_{l,m,n} \frac{\delta_{\mathbf{k}}^S \mathbf{k}}{k^2} e^{i\mathbf{k}\cdot\mathbf{x}}. \quad (2.2)$$

These displacements are readily computed on a grid using an FFT. The removal of long-wavelength power from the N-body simulation is then achieved by subtracting these displacements from the final N-body particle positions

$$\mathbf{x}' = \mathbf{x} - \mathbf{d}^S(\mathbf{x}) \quad (2.3)$$

and velocities

$$\mathbf{v}' = \mathbf{v} - f(\Omega) \mathbf{d}^S(\mathbf{x}). \quad (2.4)$$

Here $f(\Omega)$ is the logarithmic derivative of the linear growth factor $D(a)$ with respect to the expansion factor a and if we use the convention that positions are measured in units of $h^{-1}\text{Mpc}$ then the velocities are in units of 100 km s^{-1} . Note that the value of the field $\mathbf{d}^S(\mathbf{x})$ needs to be smoothly interpolated from the grid on which it is defined to each particle position.

Normally, when using the Zel'dovich approximation for a particle at position \mathbf{x} , one computes the displacement $\mathbf{d}^S(\mathbf{q})$ evaluated at the Lagrangian or starting position, \mathbf{q} , of that particle. Here instead we have deliberately computed the displacement $\mathbf{d}^S(\mathbf{x})$ at the final position \mathbf{x} . For this reason the above procedure to remove the long-wavelength

power is not exact. However, provided the displacements $\mathbf{d}^S(\mathbf{x})$ are small compared to the wavelength of the modes comprising $\Delta^S(\mathbf{x})$ the difference between $\mathbf{d}^S(\mathbf{q})$ and $\mathbf{d}^S(\mathbf{x})$ is small and approximation works quite accurately. This constraint is identical to requiring $\langle |\Delta^S(\mathbf{x})|^2 \rangle \ll 1$, as $\Delta^S(\mathbf{x}) = \nabla \cdot \mathbf{d}^S(\mathbf{x})$, and so is well satisfied in all cases of interest. Tormen & Bertschinger (1996) describe a more elaborate and accurate method of removing the long-wavelength power. The reason for deliberately using $\mathbf{d}^S(\mathbf{x})$ in equations (2.3) and (2.4) is that we do not wish to disturb the small scale structure of the N-body simulation. For example, we wish the effect of the displacement field on a dense virialized cluster to be to move the whole cluster but not disrupt its internal structure. Thus the variation of displacement $\mathbf{d}^S(\mathbf{x})$ across the cluster should be small. With the above formulation this occurs naturally as the cluster particles span only a small range in \mathbf{x} , but the shear would be considerably larger if $\mathbf{d}^S(\mathbf{q})$ were used since the cluster particles span a much larger volume in the initial Lagrangian space.

The simulation, now with no power in long-wavelength modes, is replicated to define particle positions and velocities in a much larger box of side $Lh^{-1}\text{Mpc}$. It is convenient to make L an odd multiple of S so that in \mathbf{k} -space the two grids have cells whose boundaries are aligned. A new Gaussian random field is generated from the required power spectrum

$$\Delta^L(\mathbf{x}) = \sum_{l,m,n} \delta_{\mathbf{k}}^L e^{i\mathbf{k}\cdot\mathbf{x}} \quad (2.5)$$

where $\mathbf{k} = (2\pi/L)(l, m, n)$ and $-N_L \leq l, m, n \leq N_L$ with $2N_L + 1 = (2N_S + 1)(L/S)$. Note that the sampling of \mathbf{k} -space is now on a much finer grid than for $\Delta^S(\mathbf{x})$. The corresponding Zel'dovich approximation displacements, defined over the whole box of size $Lh^{-1}\text{Mpc}$, are given by

$$\mathbf{d}^L(\mathbf{x}) = \sum_{l,m,n} \frac{\delta_{\mathbf{k}}^L \mathbf{k}}{k^2} e^{i\mathbf{k}\cdot\mathbf{x}}. \quad (2.6)$$

These are then simply added to the previous positions and velocities,

$$\mathbf{x}'' = \mathbf{x}' + \mathbf{d}^L(\mathbf{x}') \quad (2.7)$$

$$\mathbf{v}'' = \mathbf{v}' + f(\Omega) \mathbf{d}^L(\mathbf{x}') \quad (2.8)$$

to produce a particle distribution with the required improved sampling of long-wavelength modes. Note that for this second stage of the algorithm to work accurately one requires $\langle |\Delta^L(\mathbf{x})|^2 \rangle \ll 1$. This is a more stringent condition than $\langle |\Delta^S(\mathbf{x})|^2 \rangle \ll 1$ as $\Delta^L(\mathbf{x})$ contains contributions from longer wavelength modes than are present in $\Delta^S(\mathbf{x})$. In practice the full algorithm works accurately if the region of k -space from which the modes are removed and then resampled is such that $\langle |\Delta^L(\mathbf{x})|^2 \rangle^{1/2} \lesssim 0.2$.

2.2 Temporal Perturbations

The addition of long-wavelength fluctuations in the initial conditions of an N-body simulation has two effects. First the long-wavelength modes produce a wave of expansion/compression which causes a large scale modulation in the initial particle displacements and velocities. Second this same wave of expansion/compression varies the local mean density around each particle, thus perturbing the local value

of the density parameter Ω . While these long-wavelength perturbations are still in the linear regime the first of these two effects has very little influence on the evolution of small scale structure. For this reason its effect can be accurately reproduced by the MAP described in Section 2.1, which applies these perturbations after the simulation has been evolved. However the second effect of modulating the local value of the density parameter does influence the evolution of small scale structure, because in a high Ω_0 universe the linear growth rate of density fluctuations, $D(a)$, grows faster than in a low Ω_0 universe. Thus where Ω_0 is locally enhanced (diminished) by the long-wavelength perturbations, clustering will take place faster (slower) than average. This effect is not reproduced by the MAP. Below we describe a procedure whereby different regions of a simulation are allowed to evolve for different times so as to mimic the effect that the long-wavelength density perturbation would have had on the linear growth factor.

To first order the addition of a long-wavelength density perturbation, $\Delta(\mathbf{x})$, perturbs the local value of the density parameter from Ω_0 to $\Omega_0(1 + \Delta(\mathbf{x}))$. Since the growth factor is also a function of time, or expansion factor, this perturbation can also be produced by a temporal perturbation. Namely, in a region where one is adding a long-wavelength density perturbation, $\Delta(\mathbf{x})$, the simulation should be allowed to evolve longer to the point where $D(a'', \Omega_0, \Lambda_0) = D(a, \Omega_0(1 + \Delta), \Lambda_0)$. Here Λ_0 is the cosmological constant. Expanding both sides of this equation in a first order Taylor series,

$$\begin{aligned} D(a, \Omega_0, \Lambda_0) & \left[1 + \frac{a'' - a}{a} \left(\frac{\partial \ln D}{\partial \ln a} \right)_{\Omega_0, \Lambda_0} \right] \\ & = D(a, \Omega_0, \Lambda_0) \left[1 + \Delta(\mathbf{x}) \left(\frac{\partial \ln D}{\partial \ln \Omega_0} \right)_{a, \Lambda_0} \right], \end{aligned} \quad (2.9)$$

which simplifies to

$$a'' \approx a \left[1 + \frac{\Delta(\mathbf{x})}{f(\Omega)} \left(\frac{\partial \ln D}{\partial \ln \Omega} \right)_{a, \Lambda_0} \right] \quad (2.10)$$

where $\Delta(\mathbf{x}) = \Delta^L(\mathbf{x}) - \Delta^S(\mathbf{x})$. For $\Lambda_0 = 0$ this reduces to

$$a'' \approx a \left[1 + \frac{\Delta(\mathbf{x})(1 - \Omega_0^{0.6})}{(1 - \Omega_0)\Omega_0^{0.6}} \right] \quad (2.11)$$

where the usual approximation $f(\Omega) \approx \Omega^{0.6}$ (e.g. Peebles 1993) has been made. While for $\Omega_0 = 1$ this reduces to simply

$$a'' \approx a [1 + 0.6 \Delta(\mathbf{x})]. \quad (2.12)$$

This procedure can be combined with the MAP described in Section 2.1 to define new particle positions and velocities

$$\mathbf{x}''(a) = \mathbf{x}(a'') - \mathbf{d}^S(\mathbf{x}(a'')) + \mathbf{d}^L(\mathbf{x}'(a'')) \quad (2.13)$$

$$\begin{aligned} \mathbf{v}''(a) = \mathbf{v}(a'') & - f(\Omega_0)\mathbf{d}^S(\mathbf{x}(a'')) \\ & + f(\Omega_0)\mathbf{d}^L(\mathbf{x}'(a'')), \end{aligned} \quad (2.14)$$

where a'' is given by (2.10) and \mathbf{x}' by (2.3). The practical problem with this procedure is that the N-body particle distributions are now required not just at one single output time but over a quite extended range. An efficient implementation requires merging the code to solve equation (2.10) with the basic N-body evolution code so that indi-

vidual particle positions and velocities are only output at the required times. In order to create catalogues spanning very large volumes it would be necessary also to merge the code to carry out the transformations (2.14) and (2.14) and apply the galaxy catalogue selection function. If this were not done the replicated output of the N-body code would be unmanageably large.

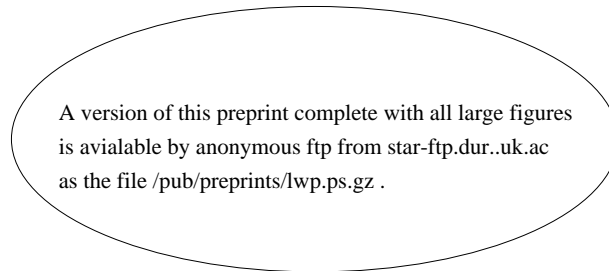
3 COMPARISON WITH FULL NON-LINEAR COMPUTATION

To test the effect of neglecting the linear to non-linear mode coupling described in Section 2.2 we now compare four sets of particle distributions derived from two N-body simulations. The first has no long-wavelength power in its initial conditions, but its evolved particle distribution is perturbed, a posteriori, using both the basic MAP detailed in Section 2.1 and the additional modification to this algorithm described in Section 2.2. The second simulation has the long-wavelength power included in the initial conditions prior to being evolved. The extent to which the basic and extended algorithms succeed can then be judged by comparing their particle distributions with that of the second simulation.

3.1 The Simulations

We first produced a realization of a Gaussian random field on a 64^3 grid with the CDM power spectrum of Bardeen *et al.* (1986) for $\Gamma \equiv \Omega_0 h = 0.25$. We chose the amplitude of the power spectrum such that the linear rms density fluctuation in spheres of radius $8h^{-1}\text{Mpc}$ was $\sigma_8 = 0.5$ at the present day, in agreement with the value required to produce the observed abundance of X-ray clusters (e.g. White, Efstathiou & Frenk 1993; Eke, Cole & Frenk 1996; Viana & Liddle 1996). The physical size of the box was chosen to be $S = 115.2h^{-1}\text{Mpc}$ and the density parameter was taken to be $\Omega_0 = 1$. The only unusual feature about this density field is that we explicitly set to zero the power in the cube of 27 modes surrounding $\mathbf{k} = 0$. Thus in the terminology of Section 2.1 we choose $N_S = 1$ and explicitly set $\Delta^S(\mathbf{x}) \equiv 0$ in this density field.

This 64^3 density field was then used to generate the initial conditions of two N-body simulations. First the density field was replicated 3^3 times to produce a periodic density field on a 192^3 grid filling a box of side $L = 3S = 345.6h^{-1}\text{Mpc}$. This density field and the Zel'dovich approximation were then used to set up a perturbed grid of 192^3 particles. The simulation evolved from these initial conditions we shall refer to as ‘‘Periodic’’. A second set of initial conditions was generated by adding a density field $\Delta^L(\mathbf{x})$ to the periodic 192^3 density field. Here $\Delta^L(\mathbf{x})$ was a Gaussian random field generated on a 192^3 , but with power only in the inner cube of 9^3 modes. Thus in the terminology of Section 2.1, $N_L = 4$ and the Fourier content of $\Delta^L(\mathbf{x})$ covers exactly that region of \mathbf{k} -space left empty in the original 64^3 density field, but on a grid which is three times finer. For the chosen power spectrum and normalization the rms value of this field is $\langle |\Delta^L(\mathbf{x})|^2 \rangle^{1/2} = 0.19$ at the final time. The simulation run from these initial conditions in which the long-wavelength density field $\Delta^L(\mathbf{x})$ was added to the particle distribution prior to evolution we shall refer



A version of this preprint complete with all large figures is available by anonymous ftp from [star-ftp.dur.uk.ac](ftp://star-ftp.dur.uk.ac) as the file `/pub/preprints/lwp.ps.gz`.

Figure 1. The mass distribution in a $5h^{-1}$ Mpc thick slice through the Prior simulation.

to as “Prior”. Both simulations were evolved from a starting redshift of $z = 4$ to the present epoch with the AP³M code of Couchman (1991), using a comoving force softening of $\eta = 180h^{-1}$ kpc (equivalent to a Plummer softening of $\epsilon = 60h^{-1}$ kpc).

A further particle distribution was generated from the first simulation by outputting the position and velocity of each particle at the time that is satisfied the equation (2.10). The long wavelength power, $\Delta^L(\mathbf{x})$, was then added to the “Periodic” and this latter distribution using the MAP to produce two final particle distributions which we refer to as “Post” and “Post+”.

3.2 The Mass Distribution

We now compare the mass distributions in the Prior and Post distributions. We note that although these simulations do not exploit the full potential of the MAP (the replicated volume contains only 64^3 particles and is replicated only 3^3 times) they provide a more direct and stringent test than the

simulations compared in Tormen & Bertschinger (1996). To the extent to which MAP works the Post and Prior particle distributions should be identical. Thus we are able to study quite subtle differences between the two simulations that would not have been possible if the two simulations had different phases and differing resolution as was the case in Tormen & Bertschinger (1996).

A visual comparison of the mass distribution in slices through the two distributions is shown in Figs. 1 and 2. The basic 3-fold periodicity of the small scale structure in the two distributions is clearly visible. However neither is strictly periodic due the presence of the long-wavelengths modes, $\Delta^L(\mathbf{x})$, present in the initial conditions of the Prior simulation and added by the MAP in the Post distribution. Clear illustrations how the MAP distorts the underlying periodic simulation are given in figures 3 and 4 of Tormen & Bertschinger (1996). On first inspection it is impressive how well the Post and Prior distributions agree. The only discernible differences are on very small scales.

To study in more detail the differences between the

A version of this preprint complete with all large figures is available by anonymous ftp from star-ftp.dur.uk.ac as the file /pub/preprints/lwp.ps.gz .

Figure 2. The mass distribution in the same slice as Fig. 1, but for the Post simulation where long-wavelength power has been added to the Periodic simulation using the Tormen & Bertschinger (1996) procedure.

Prior and Post distributions and also the Post+ distribution we plot, in Fig. 3 expanded views of two different regions. The region plotted in the left-hand panels is approximately centred on the location where the long-wavelength density field $\Delta^L(\mathbf{x})$ has its maximum, while the panels on the right are at centred on its minimum. For the left hand panels, comparing the Prior distribution (top) to Post distribution (middle) we see that the Prior distribution appears more evolved and consists of larger denser clumps. The converse is true for the Prior and Post distributions shown in the right-hand panels. This is in accord with idea that in regions where $\Delta^L(\mathbf{x})$ is positive (negative) structure has evolved more rapidly (slowly) in the Prior simulation relative to the Periodic or Post simulation. The extent to which the modification of the MAP algorithm, in which particles have been output from the N-body simulation at different times, has succeeded in reproducing this evolution can be judged by studying the bottom two panels of Fig. 3. Although not identical, the correspondence between the Post+ and Prior

distributions is very good and much better than that between Post and Prior.

The close-up inspection of two of the most extreme regions in the simulations has revealed clear differences between the Post and Prior particle distributions. However these regions are not at all typical and the impact of these differences on statistical properties of the two distributions needs to be assessed. We now use the power spectra and correlation functions of the mass distributions to quantitatively compare the large and small scale clustering in the simulations. Fig. 4 shows the mass power spectra of the four particle distributions. The power spectra were estimated using an FFT and then averaged in shells. Normally, one would average the power in spherical shells, but here we have chosen to average the power in cubical shells so as to match the geometry of the region of \mathbf{k} -space in which the long-wavelength power has been added. (The oscillations present in the equivalent figure (fig. 8) of Tormen & Bertschinger (1996) have been avoided by re-binning the power into bins

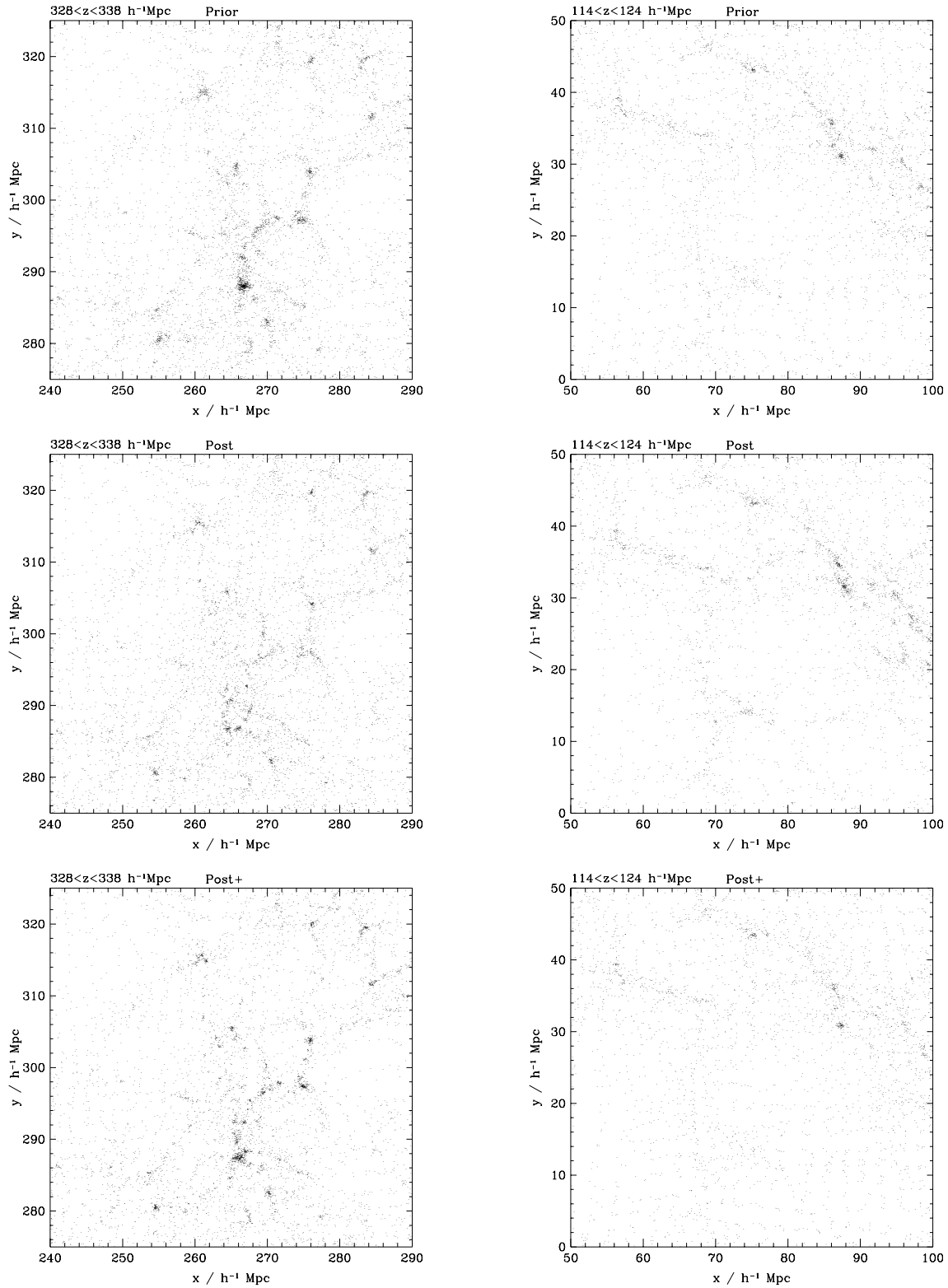


Figure 3. The left hand column of panels show small slices of the Prior, Post and Post+ simulations approximately centred on the position where the long-wavelength density field, $\Delta^L(\mathbf{x})$, has its maximum. The panels in the right-hand column are approximately centred on the position where $\Delta^L(\mathbf{x})$, has its minimum.

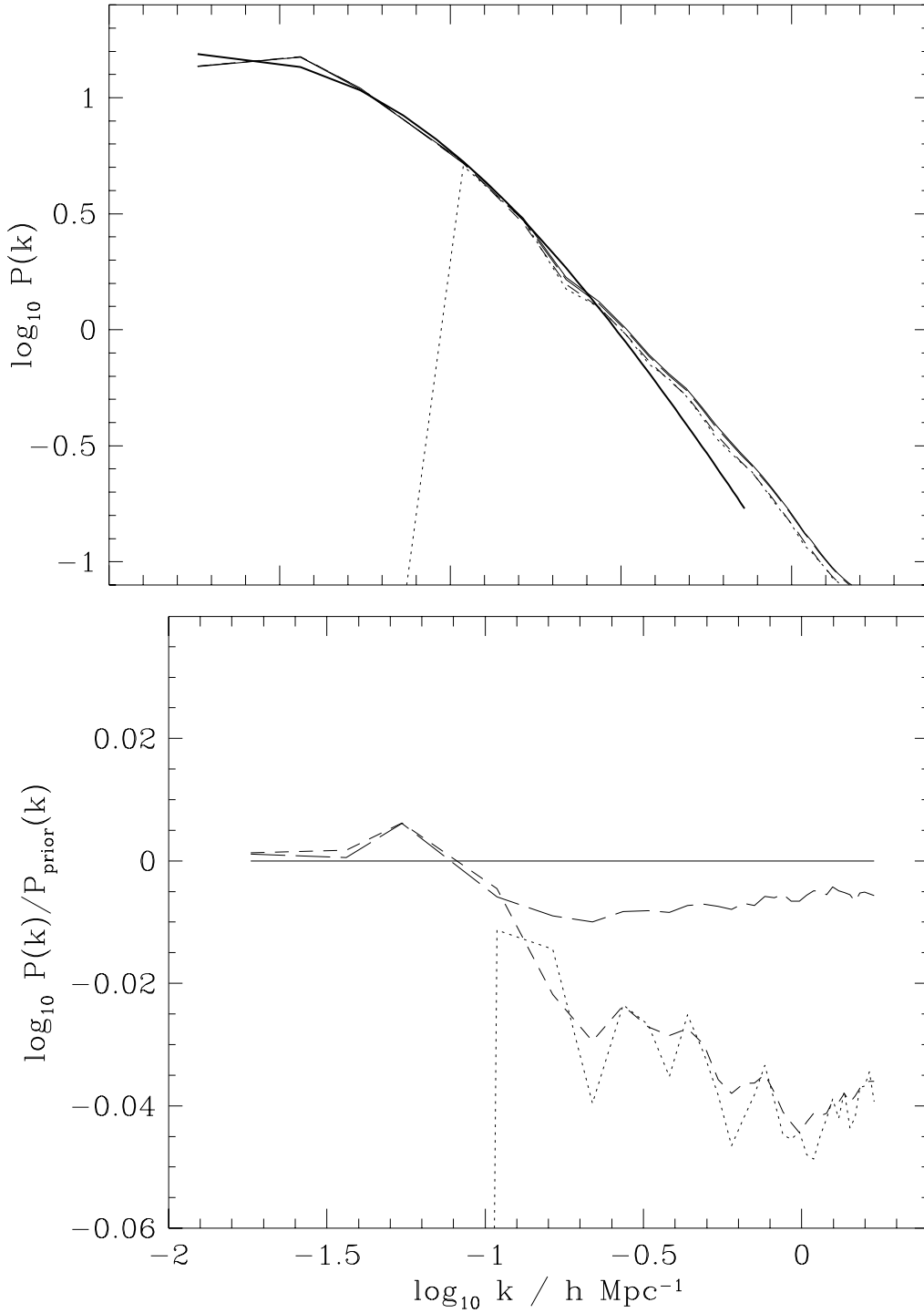


Figure 4. The mass power spectrum, $P(k)$, in the Prior (solid), Periodic (dotted), Post (short-dashed) and Post+ (long-dashed) particle distributions. The upper panel show the $P(k)$, while the lower panel shows the ratio of the various $P(k)$ to that of the Prior distribution. Also in the upper panel, the heavy solid curve shows the linear theory power spectrum. Note, the Post (short-dashed) curve is almost coincident with the Prior (solid) curve at small k , but closer to the Periodic (dotted) curve at high k . In the lower panel at high k the Periodic curve (dotted) can be seen to oscillate around Post curve (short-dashed). These small oscillations are probably an artifact of the way in which the power spectra have been binned. Each power spectrum has been averaged in cubical shells of side $2k$ and thickness matched to the sampling of \mathbf{k} -space in the initial conditions of the simulations.

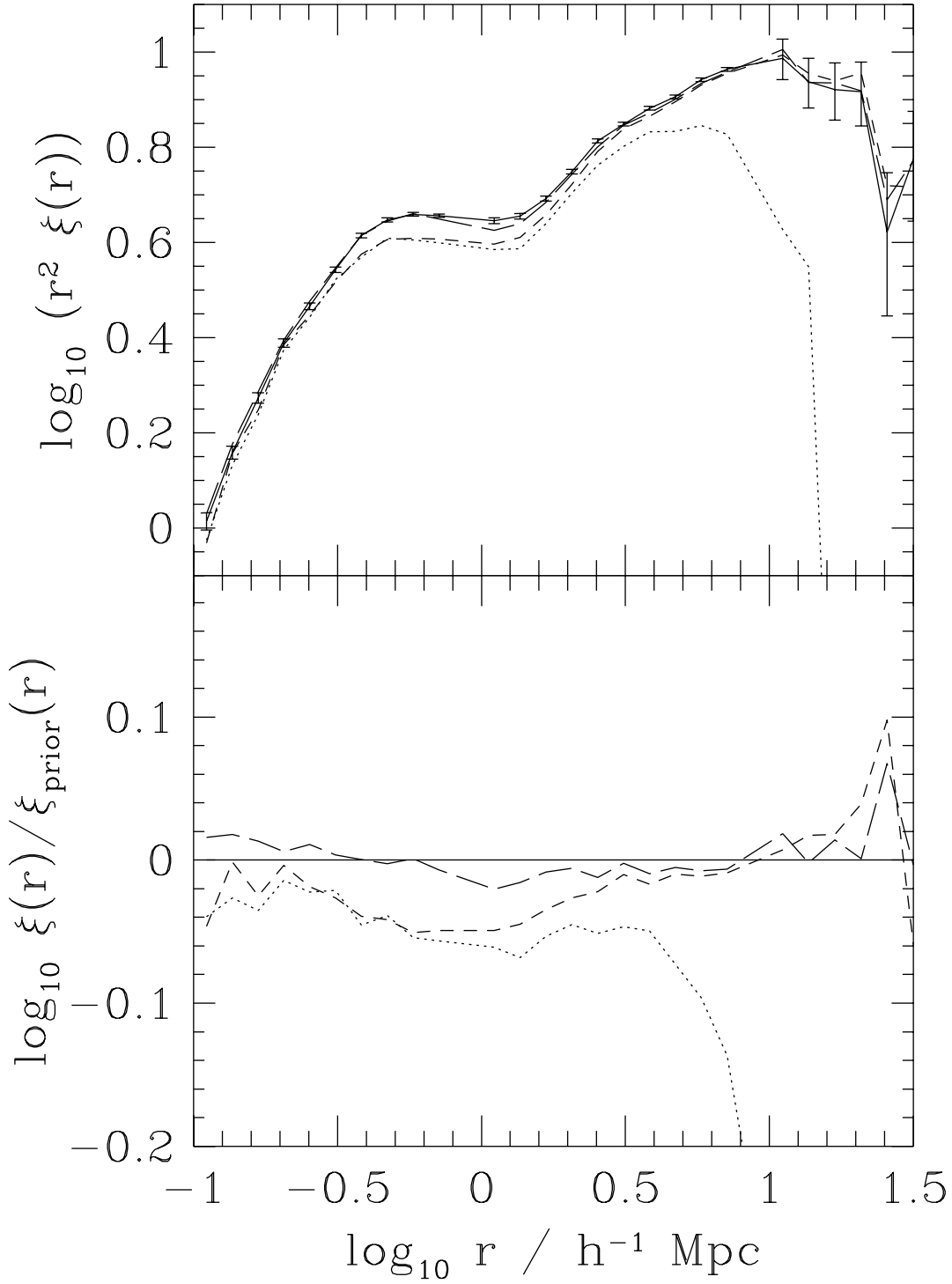


Figure 5. The upper panel show the mass correlation function, $r^2\xi(r)$ estimated from random samples of particles taken from the Prior (solid), Periodic (dotted), Post (short-dashed) and Post+ (long-dashed) particle distributions. Poisson error bars are indicated on the correlation function of the Prior simulation. The lower panel shows the ratio of the various $\xi(r)$ to that of the Prior distribution so that the differences between the distributions can be seen more clearly.

whose spacing matches the sampling of \mathbf{k} -space in the initial conditions.) The first thing to note is the sharp drop to zero power at $k < 0.11h\text{Mpc}^{-1}$ in the case of the Periodic simulation. This corresponds precisely to the region of \mathbf{k} -space in which the power spectrum was set to zero in the initial conditions of the Periodic simulation. At these same long-wavelengths the power spectra of the Post and Prior simulation track each other very accurately and scatter around the required linear theory power spectrum. At higher- k (smaller scales), all three power spectra lie above the linear theory power spectrum. Here the power spectrum of the Post simulation lies closest to that of the Periodic, which is slightly below that of the Post+ and Prior simulations. These differences can be seen much more clearly in the lower panel, which plots the ratio of the various power spectra with respect to that in the Prior simulation.

We can study the small structure in more detail by examining the correlation functions of the four distributions shown in Fig. 5. The upper panel plots $r^2\xi(r)$ rather than $\xi(r)$ so that an expanded scale can be used to reveal the quite modest differences between the various correlation functions. These differences are then high-lighted in the lower panel which plots the ratio of the various $\xi(r)$ to that of the Prior distribution. The lack of large scale power in the Periodic simulation can be seen here as a dramatic decrease in $\xi(r)$ for $r \gtrsim 10h^{-1}\text{Mpc}$. The correlation function of the Post simulation agrees well with the Prior simulation on these large scales. At smaller scales, the Post correlation function peels away from that of the Prior and matches accurately the correlation function of the Periodic simulation. The correlation function of the Post+ distribution lies close to that of the Prior distribution. This is a convincing demonstration that the basic MAP has essentially worked. The small scale structure in the Periodic simulation has been undisturbed while at the same time the required large scale power has been generated. The only sign of the neglect of the interaction between large scale linear modes and small scale structure is the slight amount by which $\xi(r)$ for the Periodic and Post simulations lies below that of the Prior simulation at small scales.

3.3 The Distribution of Clusters

Here we examine the clustering of a set of objects which do *not* simply trace the mass distribution, but are instead biased tracers. As an example of such objects we use massive groups or clusters identified in the simulations. These are strongly biased with respect to the underlying mass distributions and thus are a demanding test of the algorithms being studied. For more typical halos, such as galaxy halos, the bias is likely to be less and differences between the Prior, Post and Post+ distributions harder to detect and quantify.

We selected a sample of clusters in each of the simulations using the standard friends-of-friends group finding algorithm (Davis *et al.* 1985) with a linking length 0.2 times the mean inter-particle separation. This algorithm approximately selects groups with mean over-density of 200. We then ranked the clusters by mass and retained the 1000 with highest mass in each simulation. This gives a sample of clusters with mean separation of $34h^{-1}\text{Mpc}$ which makes them approximately three times more abundant than Abell $R \geq 1$ galaxy clusters. Slices through these cluster samples

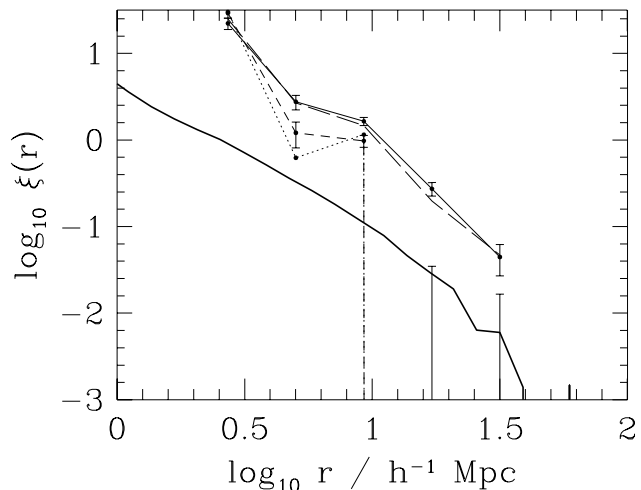


Figure 7. The cluster correlation function, $\xi(r)$, for the Prior (solid), Periodic (dotted), Post (short-dashed) and Post+ (long-dashed) distributions. Poisson error-bars are indicated on both the Post and Prior correlation functions. The lower heavy solid line shows the correlation function of the underlying mass distribution taken from the Prior simulation.

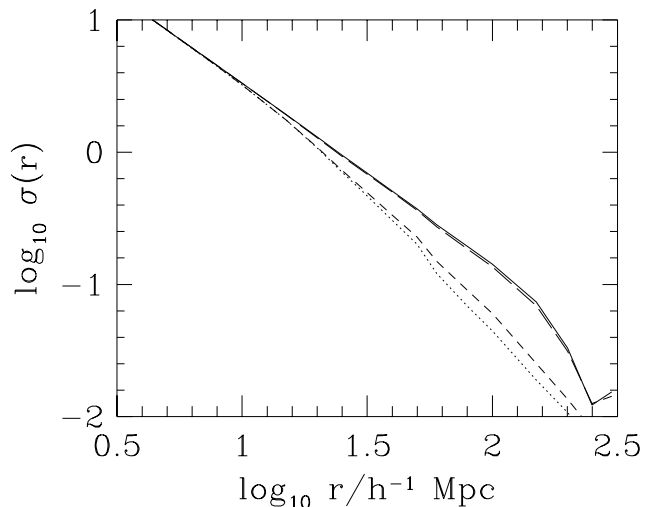


Figure 8. The rms variation, $\sigma(r)$ in the number of clusters in spheres of radius r for the Prior (solid) Periodic (dotted), Post (short-dashed) and Post+ (long-dashed) distributions. Note the Prior (solid) and Post+ (long-dashed) curves are nearly coincident on at all scales.

are shown for the Prior, Post and Post+ distributions in Fig. 6.

In many cases the same cluster is identified in all three distributions. There are some mismatches where clusters in the Prior distribution are not found in either the Post or Post+ distributions. In general the Post+ results match best with the Prior Cluster distribution. The most significant difference is the tendency for the large voids in the Prior and Post+ cluster distribution to be peppered with one or two isolated clusters in the Post distribution. This can result in a large difference in their large scale clustering properties.

We examine the clustering properties of the three cluster samples in Figs. 7 and 8. The cluster samples are too

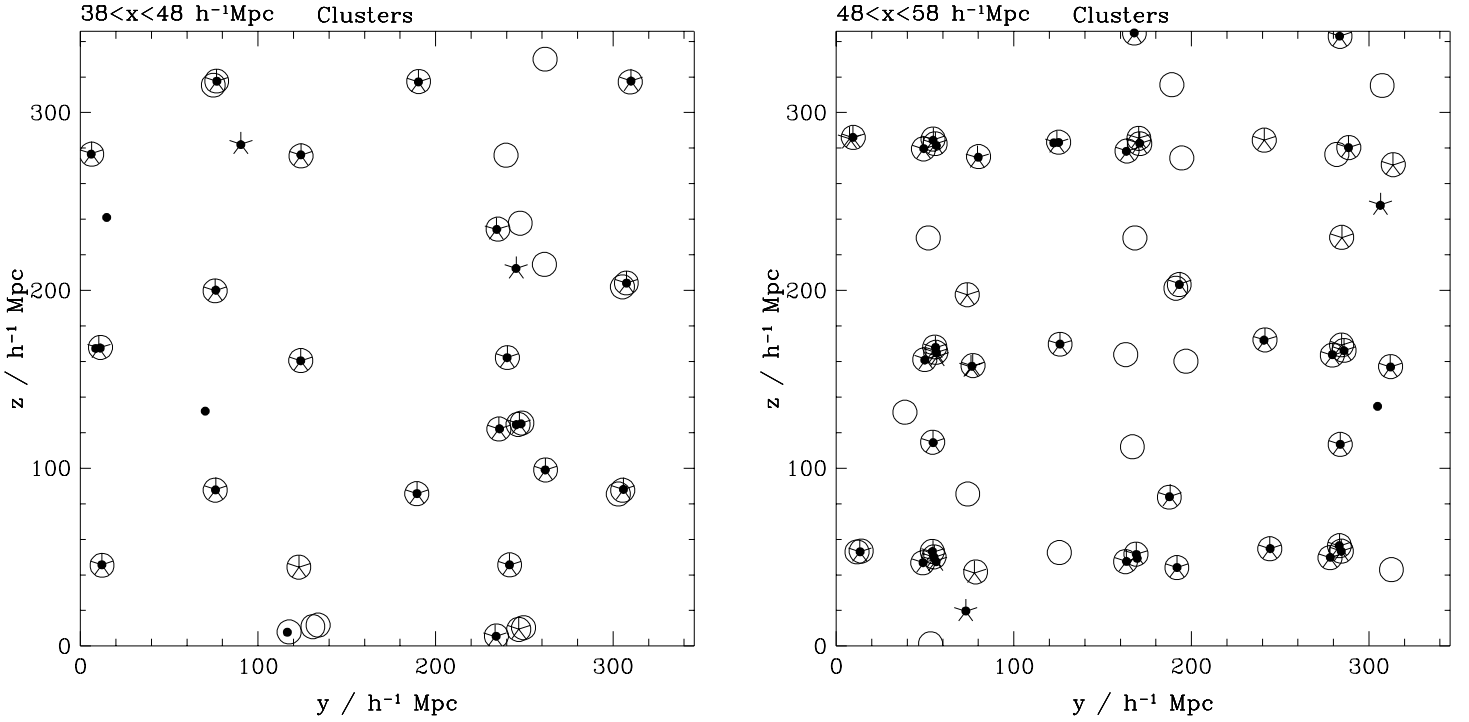


Figure 6. A comparison of the spatial distribution of galaxy clusters as defined by the friends-of-friends group finding algorithm in two slices through the Post (open circles), Prior (filled circles) and Post+ (stars) simulations. Each slice is $10h^{-1}\text{Mpc}$ thick and the left-hand slice encloses the slices of the mass distributions shown in Figs. 1 and 2

small to estimate $\xi(r)$ on very small scales. On large scales we see that the cluster correlation function in the Prior distribution is of the same shape as that of the underlying mass distribution but is offset in amplitude. In contrast the cluster correlation function in the Post simulation is considerably weaker. The correlation function for the Post+ distribution agrees well with that of the Prior cluster distribution on all scales. The differences in clustering on large scales are perhaps more clearly seen in Fig 8, which plots the fractional rms variation in the number of clusters in spheres as a function of radius, r .

Another comparison of the properties of the cluster samples is given by the peculiar velocity distribution shown in Fig. 9. In the Prior, Post and Post+ distributions the large-scale velocity fields are very almost equal. Nonetheless, differences in the peculiar velocity distributions could arise because of the differing way the cluster populations sample the velocity field in the two simulations. The similarity of the Post and Prior distributions shown in Fig. 9 indicate that this is a small effect in this case, but it is hard to dismiss in general. Also note that the peculiar velocity distribution in the Periodic simulation is much narrower. This demonstrates that long-wavelength modes produce a large contribution to the peculiar velocity and their effect is well modelled using the MAP.

The differences we have found in the properties of the cluster distributions are due to the way long-wavelength modes modulate the cluster abundance and in general the properties of the non-linear density field. In the Prior simulation the cluster abundance is modulated by, and in phase with, the long-wavelength modes in the simulation. In contrast in the Post simulation the cluster abundance is uncor-

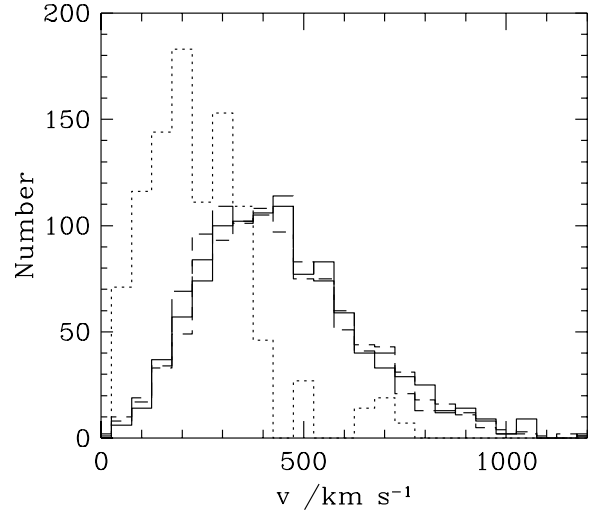


Figure 9. The peculiar velocity distributions in the Prior (solid), Periodic (dotted), Post (short-dashed), and Post+ (long-dashed) cluster distributions.

related with the long-wavelength modes which are added in after the simulation is evolved. This modulation of the cluster abundance is recovered well by the additional procedure, described in Section 2.2, incorporated in the Post+ model.

4 MOCK GALAXY CATALOGUES

The differences that we have noted in the cluster catalogues arise because the basic MAP does not produce the correct correlation between the large-scale density field and the small-scale non-linear structure. This results in large differences on large scales for the clusters, because the cluster selection is done using the small-scale properties of the non-linear density field. The same problems will also occur when constructing mock galaxy catalogues where the galaxy identification or biasing algorithm is a function of the small-scale non-linear density field. Although the magnitude of the problem may be much less if the galaxy population is not intrinsically strongly biased with respect to the mass distribution. An example of where the resulting error is important is in the determination of the density parameter Ω_0 from redshift space distortions of the clustering pattern (Kaiser 1987). At large scales, in the linear regime, a distortion is expected whose strength is determined by $\Omega_0^{0.6}/b$ and which is independent of scale. For galaxy catalogues constructed from the density produced by the basic MAP the bias parameter b will be a decreasing function of scale. Thus in the mock catalogues one would measure a distortion which indicates that $\Omega_0^{0.6}/b$ increases with scale rather than converging to the true value.

As demonstrated by the Post+ simulation presented above these problems with the basic MAP can be largely remedied by the additional procedure described in Section 2.2. However, simpler procedures maybe valuable for the specific case of creating mock galaxy catalogues. One possibility is to use the MAP as normal but select galaxies in the *initial* conditions, *i.e.* from the initial density field including the added long-wavelength contribution $\Delta(\mathbf{x}) = \Delta^L(\mathbf{x}) - \Delta^S(\mathbf{x})$. An example of defining galaxies in the initial conditions, which has been much used, is the peaks biasing scheme (White *et al.* 1987). Here the long-wavelength modes influence the galaxy selection probability through the way they modulate the number density of high peaks in the small scale density field (Bardeen *et al.* 1986). This effectively by-passes main deficiencies of the MAP. A second and more flexible approach (Tormen private communication) is to select galaxies in the non-linear density field before applying the MAP and explicitly measure their bias, b , with respect to the large scale density field. One then applies the MAP but boosts the displacements in equations (2.3) and (2.8) by the bias factor b . The perturbations to the velocities are not altered. Galaxies catalogues generated using either of these two methods will have the correct bias on large scales. Thus like the mass distribution the only error in using the MAP is then small and confined to small scales.

Clusters identified in the galaxy distribution will suffer fewer problems than those selected in the mass distribution. For example if either of the two methods proposed above are used to define galaxy catalogues in the Post and Prior simulations then the number of galaxies selected in volumes illustrated in the two top right-hand panels of Fig. 3 should be the same. Statistically, the only way in which the galaxy catalogue generated in the Post simulation will differ from that in the Prior simulation is in their velocity fields. In the region shown the Prior simulation has a quieter or cooler velocity field than the more evolved region in the Prior sim-

ulation. Since the region shown in this figure is only 0.05% of the volume of the whole simulation and is likely to be the most extreme example of this type of difference it is unlikely to be important for nearly all applications of mock galaxy catalogues.

5 CONCLUSIONS

The algorithm devised by Tormen & Bertschinger (1996) allows the dynamic range of N-body simulations to be extended to very large scales by adding to them linear power on very large scales. However, the Tormen & Bertschinger (1996) Mode Adding Procedure (MAP) neglects coupling between long-wavelength linear modes and short-wavelength non-linear modes. This coupling arises through the way long-wavelength density modes modulate the rate of evolution of small scale structure. Although the amplitude of this effect is small it is of the same order as the amplitude of the long-wavelength density modes. Thus for objects such galaxy clusters and perhaps galaxies identified in the non-linear density field the neglect of this coupling leads to a large error in the amplitude of their large-scale clustering pattern. On the other hand, for the mass distribution as a whole we find the basic MAP works very accurately with essentially no error in the mass correlation function on large scales and only a small error in the amplitude on small scales.

The main short-comings of the MAP can be avoided by two methods. The first is to select objects in the initial conditions where the initial conditions include the long-wavelength modes that are to be introduced using the MAP of Tormen & Bertschinger (1996). The second is to boost displacements, but not the velocity perturbations, applied by the MAP to take account of the known bias, b of the selected population of objects. Thus mock galaxy catalogues generated by either of these methods will benefit from the ability of the MAP to better sample modes of the very large scale density field. Alternatively, if one requires the full mass distribution then the Tormen & Bertschinger procedure can be extended to explicitly address the coupling of long-wavelength modes to small scale structure by using multiple outputs from the evolving N-body simulation as described in Section 2.2.

ACKNOWLEDGEMENTS

SMC would like to thank Carlos Frenk for useful discussions and Hugh Couchman for providing a copy of his AP³M N-body code and giving valuable advice. SMC also gratefully acknowledges the support of a PPARC Advanced Fellowship.

REFERENCES

- Bardeen, J.M., Bond, J.R., Kaiser, N., Szalay, A.S., 1986, ApJ, 304,15
- Couchman, H.M.P., 1991, ApJ.Lett, 368,23
- Davis, M., Efstathiou, G., Frenk, C.S., White, S.D.M., 1985, ApJ, 292,371
- Eke, V.R. Cole, S. Frenk, C.S., 1996, MNRAS 282,263
- Gunn, J.E. 1995 BAAS, 186,44

- Kaiser, N., 1987, MNRAS, 227,1
Peebles, P.J.E., 1993, Principles of Physical Cosmology. Princeton University Press, Princeton, NJ.
Tormen , G., Bertschinger, E., 1996, ApJ, 472,
Viana, P.T.P., Liddle, A.R., 1996, MNRAS 281, 323
White, S.D.M., Davis, M., Efstathiou, G., Frenk, C.S., 1987, Nature, 330,451
White, S.D.M., Efstathiou, G., Frenk, C.S. 1993, MNRAS, 262,1023
Zel'dovich Y.B., 1970, A& A 5,84